

---

# GBA: A Tuning-free Approach to Switch between Synchronous and Asynchronous Training for Recommendation Models

---

Wenbo Su\*, Yuanxing Zhang\*, Yufeng Cai, Kaixu Ren, Pengjie Wang, Huimin Yi,  
Yue Song, Jing Chen<sup>1</sup>, Hongbo Deng, Jian Xu, Lin Qu<sup>1</sup>, Bo Zheng<sup>†</sup>

Alibaba Group

{vincent.swb, yuanxing.zyx, baike.cyf, kaixu.rkx,  
pengjie.wpj, huimin.yhm, yue.song, dhb167148,  
xiyu.xj, bozheng}@alibaba-inc.com  
<sup>1</sup>{gongcheng.cj, xide.ql}@taobao.com

## Abstract

High-concurrency asynchronous training upon parameter server (PS) architecture and high-performance synchronous training upon all-reduce (AR) architecture are the most commonly deployed distributed training modes for recommendation models. Although synchronous AR training is designed to have higher training efficiency, asynchronous PS training would be a better choice for training speed when there are stragglers (slow workers) in the shared cluster, especially under limited computing resources. An ideal way to take full advantage of these two training modes is to switch between them upon the cluster status. However, switching training modes often requires tuning hyper-parameters, which is extremely time- and resource-consuming. We find two obstacles to a tuning-free approach: the different distribution of the gradient values and the stale gradients from the stragglers. This paper proposes Global Batch gradients Aggregation (GBA) over PS, which aggregates and applies gradients with the same global batch size as the synchronous training. A token-control process is implemented to assemble the gradients and decay the gradients with severe staleness. We provide the convergence analysis to reveal that GBA has comparable convergence properties with the synchronous training, and demonstrate the robustness of GBA the recommendation models against the gradient staleness. Experiments on three industrial-scale recommendation tasks show that GBA is an effective tuning-free approach for switching. Compared to the state-of-the-art derived asynchronous training, GBA achieves up to 0.2% improvement on the AUC metric, which is significant for the recommendation models. Meanwhile, under the strained hardware resource, GBA speeds up at least 2.4x compared to synchronous training.

## 1 Introduction

Nowadays, recommendation models with a large volume of parameters and high computational complexity have become the mainstream in the deep learning communities [12]. Accelerating the training of these recommendation models is a trending issue, and recently synchronous training upon high-performance computing (HPC) has dominated the training speed records [16, 15, 29]. The resource requirements of the synchronous training upon AR are more rigorous than the asynchronous

---

\* \* These authors contributed equally to this work.

<sup>†</sup> † Corresponding author

training upon PS [1]. In a shared training cluster with dynamic status [2], the synchronous training would be retarded by a few straggling workers. Thus, its training speed may be even much slower than the high-concurrency asynchronous training.

Should it be possible to switch the training mode according to the cluster status, we will have access to making full use of the limited hardware resources. Switching the training mode for a specific model usually demands tuning of the hyper-parameters for guarantees of accuracy. Re-tuning the hyper-parameters is common in the one-shot training workloads (e.g., the general CV or NLP workloads) [18]. However, it is not applicable for the continual learning or the lifelong training of the recommendation models [9], as tuning would be highly time- and resource-consuming. When switching the training mode of representative recommendation models, we confront three main challenges from our shared cluster: 1) Model accuracy may suffer from a sudden drop after switching, requiring the model to be retrained on a large amount of data to reach the comparable accuracy before switching; 2) The distribution of gradient values is different between synchronous training and asynchronous training, making the models under two training modes difficult to reach the same accuracy by tuning the hyper-parameters; 3) The cluster status imposes staleness on the asynchronous training, and staleness negatively impacts the aggregation of gradients, especially for the dense parameters.

We conduct a systematic investigation of the training workloads of recommendation models to tackle the above challenges. It is found that when the global batch size (i.e., the actual batch size of gradient aggregation) is the same, the distribution of gradient values of asynchronous training tends to be similar to that of synchronous training. Besides, we notice that due to the high sparsity, the embedding parameters in recommendation models are less frequently updated than the dense parameters, leading to a stronger tolerance for staleness than the general CV or NLP deep learning models. Based on these insights, we propose Global Batch gradients Aggregation (GBA), which ensures the model keeps the same global batch size when switched between the synchronous and asynchronous training. GBA is implemented by a token-control mechanism, which resorts to bounding the staleness and making gradient aggregation [11]. The mechanism suppresses the staleness following a staleness decay strategy over the token index. The faster nodes would take more tokens without waiting, and thereby GBA trains as fast as the asynchronous mode. Furthermore, the convergence analysis shows that GBA has comparable convergence properties with the synchronous mode, even under high staleness for recommendation models. We conduct an extensive evaluation on three continual learning of recommendation tasks. The results reveal that GBA performs well on both accuracy and efficiency with the same hyper-parameters. Particularly, GBA improves the AUC metric by 0.2% on average compared to the state-of-the-art training modes of asynchronous training. Besides, GBA presents at least 2.4x speedup over the synchronous AR training in the cluster with strained hardware resources.

To the best of our knowledge, this is the first work to approach switching between synchronous and asynchronous training without tuning the hyper-parameters. GBA has been deployed in our shared training cluster. The tuning-free switching enables our users to dynamically change the training modes between GBA and the synchronous HPC training for the continual learning tasks. The overall training efficiency of these training workloads is thereby significantly improved, and the hardware utilization within the cluster is also raised by a large margin.

## 2 Related Work

**Distributed training mode.** PS [19] and AR [16] are two mainstream architectures for the training workloads of recommendation models, accompanied by the asynchronous training and synchronous training, respectively. Researchers are enthusiastic about the pipeline, communication, and computation optimization for the AR architecture of recommender systems [29]. Meanwhile, to improve the training efficiency of the PS architecture, researchers propose a category of *semi-synchronous* training mode [11]. For example, Hop-BS [22] restricts the gradient updates under the bounded staleness, and Hop-BW [22] ignores the gradients from the stragglers with the well-shuffled and redundancy data. Recently, a category of *decentralized training* has been proposed in many studies to scale out the AR architecture. Local all-reduce [23], local update [24], exponential graph [26], and many topology-aware solutions have proven promising in the NLP and CV tasks. However, owing to the sparsity in recommendation models, the inconsistent parameters among workers and the dropped gradients of the scarce IDs would intolerably degrade the accuracy. Besides, these training modes

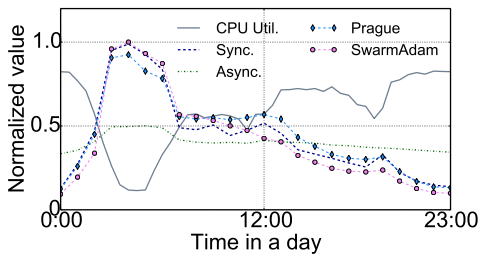


Figure 1: Normalized QPS of four training modes in training YouTubeDNN models in a shared cluster, with CPU utilization in a day.

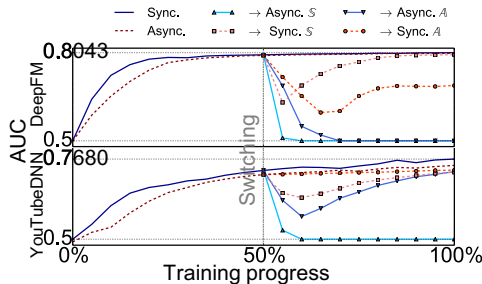


Figure 2: The AUC on the validation set of Criteo-4GB and Private by every 5% progress during training, switching at 50% progress.

hardly consider the requirements to switch to another training mode according to the cluster status, though switching is beneficial to improve the training efficiency in the shared training clusters.

**Staleness and noisy gradients.** The indeterminate or even inferior model accuracy of asynchronous training is mainly attributed to the staleness [6] and the noisy gradients [25] caused by the small batch. Although prior research has pointed out that the converged giant model is less sensitive to staleness [7], staleness is still a negative factor in the accuracy of the continual recommendation training. Many efforts have been put into controlling staleness via Taylor expansion [30], weighted penalty [33], etc. Recent works present a large-batch training paradigm with specially-designed optimizers to scale the gradients before updating [27], and point out that it can reach the best accuracy by merely adjusting batch size [10, 28]. There are also attempts to change gradient aggregation strategies during the asynchronous training to achieve stable model accuracy [20]. GBA generalizes the staleness control paradigm to the recommendation workloads by token-control mechanism, which finds the balance between bounding staleness and ignoring gradients. GBA runs with the same global batch size as the synchronous mode, ensuring the effective switching between GBA and synchronous training without tuning hyper-parameters.

### 3 Preliminaries

#### 3.1 Distributed Training of Recommendation Models

Recommendation models usually comprise two modules: the *sparse* module contains the embedding layers with the *embedding parameters*, mapping the categorical IDs into numerical space; the *dense* module contains the computational blocks with the *dense parameters*, such as attention and MLP [3, 31], to exploit the feature interactions. The main difference between the two kinds of parameters is the occurrence ratio in each training batch. Each training batch needs all the dense parameters, yet only a tiny amount of embedding parameters are required according to the feature IDs in the data shard. The latest development of recommendation models introduces high complexity and a large volume of parameters, making distributed training essential to improve training efficiency. The synchronous HPC training mode usually adopts the AR architecture, where the dense parameters are replicated, and the embedding parameters are partitioned on each worker. HPC should be deployed by monopolizing a few high-performance workers and making full use of the associated resources, which may be retarded by the slow workers [17]. PS architecture is usually coupled with asynchronous high concurrency training where the parameters are placed on PSs, and the workers are responsible for the computation. On the one hand, the high concurrency mechanism activates the fragmentary resources in the training cluster by deploying hundreds of workers. On the other hand, the asynchronous training brings in *gradient staleness*, which occurs when the gradient is calculated based on the parameters of an old version and applied to the parameters of a new version.

#### 3.2 Observations and Insights within a Shared Training Cluster

We investigate the training workloads of recommendation models from a shared training cluster to observe the obstacles and necessities of switching training modes.

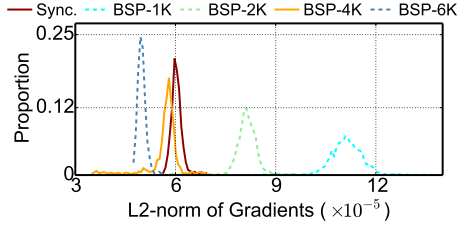


Figure 3: The distribution of L2-norm of gradients from the synchronous training and BSP with various size of aggregation.

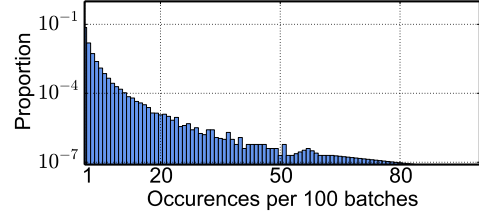


Figure 4: The skewed distribution of ID occurrences across batches, reflecting the frequency that an ID gets updated.

**Observation 1: Cluster status determines the performance of training modes.** Figure 1 illustrates the average CPU utilization within a real shared cluster, and the corresponding samples/queries per second (QPS) of a YouTubeDNN [5] model by the synchronous and asynchronous training mode. The utilization and QPS are normalized by their maximal value, respectively. When the cluster is relatively vacant, models trained in the synchronous mode can fully occupy the hardware resources, satisfying HPC conditions and presenting high efficiency. When there are plenty of heterogeneous workloads in the cluster, slow workers dominate the training speed, making the asynchronous training mode run much faster than the synchronous mode. We also implement two approaches of local all-reduce<sup>3</sup>. Since the status of each device in the cluster is constantly changing, the local all-reduce-based mode would not work well when confronting resource shortages.

**Observation 2: Directly switching training mode brings sudden drop on accuracy.** We run DeepFM [21] over Criteo-4GB [14] (few parameters, fast convergence) and YouTubeDNN on Private dataset (trillions of parameters, slow convergence) in the shared cluster. We tune the hyper-parameters from scratch for the best model accuracy of both asynchronous and synchronous mode, and denote the two sets of hyper-parameters as set  $\mathbb{A}$  and set  $\mathbb{S}$ , respectively. After training in one training mode, we evaluate the tendency of the training AUC after switching to the other training mode with set  $\mathbb{A}$  or set  $\mathbb{S}$ . Figure 2 illustrates that after switching from the synchronous mode to the asynchronous mode, the AUC encounters sudden drop and even decreases to 0.5. The AUC drop also appears in the opposite-side switching, indicating that this condition is irrelevant to whether the model had been converged. These observations imply that directly switching the training mode requires heavy effort in re-tuning the hyper-parameter. Inherently, training modes would lead to different convergence or minima owing to the difference in batch size, learning rate and many other factors, which have already received in-depth theoretical research [? ?]. We provide theoretical analysis to explain the sudden drop in Appendix D.

We then probe into the insights from asynchronously training recommendation models.

**Insight 1: Distribution of the gradient values is related to the aggregated batch size.** We attempt to investigate the reason for observation 2 from the gradient aspect. We implement asynchronous bulk synchronous parallel (BSP) on the YouTubeDNN recommendation task, which asynchronously aggregates  $K$  gradients from workers before applying the values to the parameters. Here, we set  $K$  to 100, the same as the number of workers. Besides, we compare the synchronous training in 6.4K local batch size (64 workers). Figure 3 plots the distribution of the L2-norm of gradient values from the synchronous training and BSP with various local batch sizes. It is evident that the batch size determines the mean and variance of the distribution. The distribution of BSP resembles synchronous training when the aggregation size is similar (i.e., BSP-4K). The result suggests that the same aggregation size could lead to a similar distribution of gradient values. However, there is still a gap in model accuracy after equalizing the global batch size between the asynchronous training and the synchronous training, mainly induced by gradient staleness.

**Insight 2: The gradient staleness imposes different impact on the embedding parameters and the dense parameters.** Due to the skewed distribution, most IDs would merely appear in a small number of batches, as depicted in Fig. 4. It means that in the recommendation models, only a tiny portion of IDs would be involved in every single batch, and the embedding parameters are less

<sup>3</sup>SwarmAdam is a variant of SwarmSGD [24] with Adam optimizer. It is uncommon to use SwarmAdam and Prague [23] in recommendation models as they may lead to accuracy loss which is not tolerable in the business.

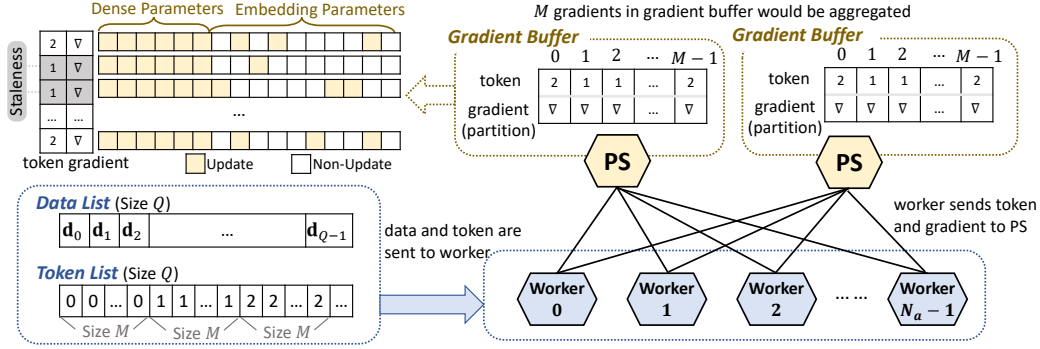


Figure 5: Illustration of the token-control mechanism in GBA: every  $M$  gradients would be aggregated in the buffer before the PSs apply them to the parameters; workers report gradients to the PSs along with a token indicating the degree of data staleness.

frequently updated than the dense parameters. Therefore, the embedding parameters tend to be more robust on the gradient staleness than the dense parameters (for example, considering a worker in training, there could be five updates for the dense parameters, yet only two updates for the embedding of a specific ID).

## 4 Global Batch based Gradients Aggregation

### 4.1 Training Recommendation Models with GBA

Switching the distributed training mode for recommendation models should get rid of tuning the hyper-parameters. We introduce the concept of *global batch size*, which is defined as the actual batch size when gradients are aggregated and applied, and propose GBA for the tuning-free switching. We denote the *local batch size*, i.e., the actual batch size on each worker and the number of workers, as  $B_s$  and  $N_s$  for the synchronous training,  $B_a$  and  $N_a$  for the asynchronous training. Then, the global batch size in synchronous training, denoted by  $G_s$ , can be calculated as  $B_s \times N_s$ . Following Insight 1, GBA remains the global batch size unchanged when we switch the distributed training model from synchronous training to asynchronous training. For each step, all the dense parameters would be updated, and only a small number of embedding parameters would be updated. Then the dense parameters and embedding parameters obtain different gradient staleness during training. Hence, we define the *data staleness* as the unified staleness in training recommendation models. The data staleness describes the gap between the global step when the worker begins to ingest a data batch and the global step when the calculated gradient is applied. Obviously, the data staleness in the synchronous training mode is constantly zero. Based on data staleness, we implement GBA by a token-control mechanism on the PS architecture to cope with the sparsity and the dynamic cluster status.

Figure 5 illustrates the architecture of the proposed token-control mechanism. Over the canonical PS, we prepare a queue called *data list* to arrange the data (addresses) by batches. Given a dataset  $\mathcal{D}$ , suppose we can split it into  $Q$  batches of size  $B_a$ , denoted by  $\mathcal{D} = (\mathbf{d}_0, \mathbf{d}_1, \dots, \mathbf{d}_{Q-1})$ . Meanwhile, we establish another queue called *token list* to yield the token of each individual batch. The token list contains  $Q$  tokens, denoted by  $(t_0, t_1, \dots, t_{Q-1})$ , each attached to one batch in the data list to indicate the global step when this batch is sent to a worker. The token value starts from zero, and each token value repeats  $M$  times in the token list. Here,  $M$  is the number of batches we use to aggregate gradients. Under this setting, we can deduce that there will be  $K = \lceil \frac{Q}{M} \rceil$  gradient updates during the training. Then we set  $t_i = \lfloor \frac{i}{K} \rfloor, \forall i \in \{0, 1, \dots, Q-1\}$  to ensure that the token list yields the token value in ascending order. Apart from the two queues, we also employ a *gradient buffer* to receive the gradients calculated by the workers with the corresponding tokens of the gradients. To be consistent with the tokens, the capacity of the gradient buffer is set to  $M$ , and therefore the PSs would aggregate  $M$  gradients before applying them to the variables. Note that each PS maintains an individual gradient buffer to deal with the gradients of the corresponding partitions of the variables.

During the training process, a worker would pull the parameters from PS, a batch from the data list, and a token from the token list simultaneously before ingesting the data and computing the gradient locally. When a worker completes calculating the gradient of a batch, the gradient and the corresponding token are sent to the gradient buffer on PS. Then, the worker immediately proceeds to work on the next batch. In this way, the fast workers can keep working without waiting for the slow ones. When the gradient buffer reaches the capacity of  $M$  pairs of gradients and tokens, all the gradients are aggregated to apply once, and at the same time, the buffer will be cleared. This is what we call finishing a global step, and thereby the global batch size in GBA can be calculated as  $G_a = B_a \times M$ . According to the design, we aim to keep the global batch size consistent in switching, that is,  $G_s = G_a$ . Hence, we can set the size of the gradient buffer to be  $M = \frac{B_s \times N_s}{B_a}$ . We would use  $M$  workers in GBA, i.e.,  $N_a = M$ , to avoid the intrinsic gradient staleness led by the inconsistency between the number of workers and the number of batches to aggregate.

At the update of global step  $k$ , denote  $\tau(m, k)$  the  $m$ -th token in the gradient buffer. When we aggregate the gradients in the gradient buffer, we shall decay the gradients that suffer from severe staleness. GBA could employ different staleness decay strategies to mitigate the negative impact from the staleness according to the token index, and in this work we define it as:

$$f(\tau(m, k), k) = \begin{cases} 0, & k - \tau(m, k) > \iota \\ 1, & k - \tau(m, k) \leq \iota, \end{cases} \quad (1)$$

where  $\iota$  is the threshold of tolerance. If  $f(\tau(m, k), k) = 0$ , we exclude the  $m$ -th gradient in the buffer due to the severe staleness; otherwise, we aggregate the gradient. As we can see, tokens help identify whether the corresponding gradients are stale and how many stale steps are behind the current global step. In this case, although the token is designed over the data staleness, the negative impact from the canonical gradient staleness can also be mitigated.

## 4.2 Convergence Analysis

We have seen much research on the convergence analysis of the synchronous and asynchronous training. Following the assumptions and convergence analysis in Dutta et al. [6], the expectation of error after  $k$  steps of gradient updates in the synchronous training can be deduced by:

$$\mathbb{E}[F(\mathbf{w}_k)] - F^* \leq \frac{\eta L \sigma^2}{2c N_s B_s} + (1 - \eta c)^k (F(\mathbf{w}_0) - F^* - \frac{\eta L \sigma^2}{2c N_s B_s}), \quad (2)$$

where  $\mathbf{w}_k$  denotes the parameter in step  $k$ ,  $\eta$  denotes learning rate,  $L$  is the Lipschitz constant and  $\sigma$  denotes the variance of gradients.  $F(\mathbf{w})$  is the empirical risk function that is strongly convex with parameter  $c$ .  $\mathbb{E}[F(\mathbf{w}_k)] - F^*$  is the expected gap of the risk function from its optimal value, used as the error after  $k$  steps. As mentioned in Eqn. (2), The first term in the right, i.e.  $\frac{\eta L \sigma^2}{2c(N_s B_s)}$ , would be the error floor, and  $(1 - \eta c)$  is the decay rate. The proposed GBA is derived upon the asynchronous gradient aggregation. We assume that, for some  $\gamma \leq 1$ ,

$$\gamma \geq \frac{\zeta \mathbb{E}[\|\nabla F(\mathbf{w}_k) - \nabla F(\mathbf{w}_{\tau(m, k)})\|_2^2]}{\mathbb{E}[\|\nabla F(\mathbf{w}_k)\|_2^2]}. \quad (3)$$

Here,  $\gamma$  is a measure of gradients impact induced by the staleness; smaller value of  $\gamma$  indicates that staleness makes less accuracy deterioration of the model. Besides,  $\zeta$  indicates the average probability that any parameter in the model would be both updated in step  $k$  and step  $\tau(m, k)$ . Intuitively,  $\zeta$  would be far below 1 in the recommendation models due to the strong sparsity. Then, the error of GBA after  $k$  steps of aggregated updates would become (Appendix A presents the proof):

$$\mathbb{E}[F(\mathbf{w}_k)] - F^* \leq \frac{\eta L \sigma^2}{2c \gamma' M B_a} + (1 - \eta \gamma' c)^k (\mathbb{E}[F(\mathbf{w}_0)] - F^* - \frac{\eta L \sigma^2}{2c \gamma' M B_a}), \quad (4)$$

where  $\gamma' = 1 - \gamma + \frac{p_0}{2}$  and  $p_0$  is a lower bound on the conditional probability that the token equals to the global step, i.e.,  $\tau(m, k) = k$ . Equation (4) proves the convergence of GBA. Considering the error floors of Eqn. (2) and Eqn. (4),  $M \times B_a$  should be set close to  $N_s \times B_s$  to make GBA tuning-free. It is exactly the global batch size we use in GBA, consistent with our main idea of keeping global batch size unchanged. Recall that with the embedding parameters,  $\zeta < 1$  makes  $\gamma$  lower than the training of general CV or NLP models. Consequently, the error floor remains low in GBA.

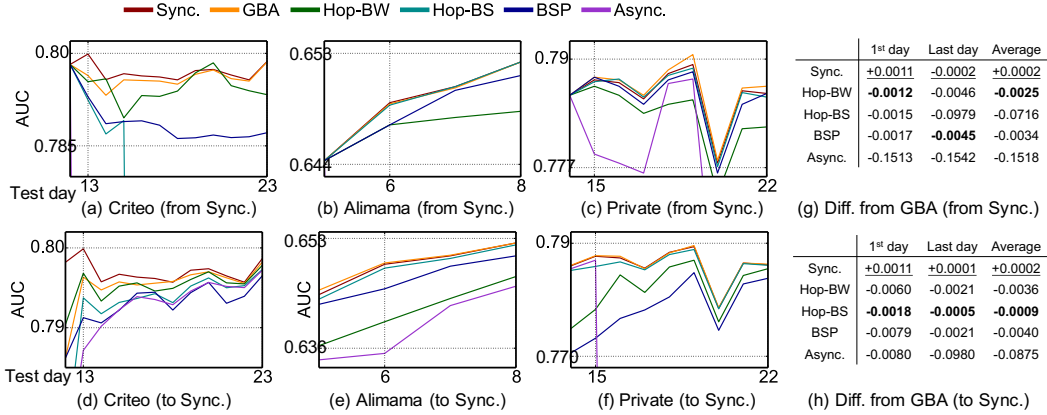


Figure 6: The AUC tendencies on the test days of the three datasets after inheriting a base model: (a-c) from the synchronous training modes and switching to the compared training modes; (d-f) from the compared training modes and switching to the synchronous training modes; (g-h) AUC difference between GBA and the other training modes after switching from/to synchronous training.

## 5 Evaluation

### 5.1 Settings

Table 5.1: Settings of the three continual recommendation tasks by the compared training modes.

Task	Model description	Data parts	Sample per day	Optimizer	Learning rate	# of workers	Local size	batch	Private hyper-param.
Criteo (DeepFM)	19M(x40K) FLOPS 45B params. 16 avg. dim.	12 days (base)	190M	Adagrad (Async.)	0.006 (Async.)	32 (Sync.)	5K (Async.)		Hop-BS ( $b_1=2$ )
		11 days (eval)		Adam (Others)	0.0011 (Others)	100 (Others)	12.8K (GBA)	BSP ( $b_2=20$ )	
Alimama (DIEN)	112M(x3K) FLOPS 160B params. 19 avg. dim.	5 days (base)	90M	Adagrad (Async.)	0.008 (Async.)	32 (Sync.)	1K (Async.)		Hop-BS ( $b_1=2$ )
		3 days (eval)		Adam (Others)	0.0015 (Others)	128 (Others)	0.75K (GBA)	BSP ( $b_2=20$ )	
Private (YouTubeDNN)	746M(x6.4K) FLOPS 1.9T params. 24 avg. dim.	14 days (base)	2B	Adagrad (Async.)	0.001 (Async.)	64 (Sync.)	1K (Async.)		Hop-BS ( $b_1=2$ )
		8 days (eval)		Adam (Others)	0.0006 (Others)	400 (Others)	1K (GBA)	BSP ( $b_2=50$ )	
							6.4K (Others)		Hop-BW ( $b_3=100$ )
									GBA ( $\iota=4$ )

We conduct systematical evaluations to examine the performance of GBA and make a fine-grained analysis. The evaluations involve three industrial-scale recommendation tasks: 1) On the Criteo-1TB dataset [13], we implement DeepFM, where the hyper-parameters on Criteo-4GB (AUC 0.8043) are utilized; 2) On the Alimama dataset [8], we implement DIEN [32] and use the recommended hyper-parameters in the original design; 3) On the Private dataset, we implement YouTubeDNN, and we tune the best hyper-parameters. The models are implemented in DeepRec [4] with the expandable HashTables. Detailed information on the dataset and the models are listed in Tab. 5.1. We imitate the continual training without changing the hyper-parameters to the models, and ensure a similar cluster status for all evaluations. Inheriting from a pre-trained checkpoint, we repeatedly train on the data of every day and evaluate the data of the subsequent day. The training cluster is equipped with a Tesla-V100S GPU and Skylake CPU. We focus on AUC as the accuracy metric and global/local QPS (QPS of all/single workers) as the efficiency metric.

We select several state-of-the-art PS-based training modes: Bounded staleness (Hop-BS) restricts the maximal differences of gradient version between the fastest and the slowest workers, controlled by  $b_1$ ; Bulk synchronous parallel (BSP) aggregates a pre-set number  $b_2$  of gradients when applying gradients to the parameters, regardless of the gradient version; Backup worker (Hop-BW) ignores the pre-set number  $b_3$  of gradients from the slowest workers during each gradient aggregation. We enumerate the specialized hyper-parameters of each training mode and record the statistics when reaching its best AUC.

Table 5.2: Global QPS of the compared training mode on the three tasks.

	Sync.	Async.	Hop-BS	BSP	Hop-BW	GBA
<b>Críteo</b>	1,436K( $\pm$ 224K)	3,253K( $\pm$ 84K)	2,227K( $\pm$ 336K)	3,247K( $\pm$ 93K)	2,559K( $\pm$ 294K)	<b>3,240K(<math>\pm</math>97K)</b>
<b>Alimama</b>	182K( $\pm$ 52K)	403K( $\pm$ 33K)	217K( $\pm$ 65K)	403K( $\pm$ 33K)	288K( $\pm$ 48K)	<b>399K(<math>\pm</math>35K)</b>
<b>Private</b>	43K( $\pm$ 21K)	90K( $\pm$ 15K)	29K( $\pm$ 11K)	88K( $\pm$ 17K)	66K( $\pm$ 24K)	<b>87K(<math>\pm</math>19K)</b>

Table 5.3: Fine-grained analysis between GBA and the other training modes.

Local QPS		AUC		# of drop		Avg. grad. staleness (max)		
Async.	GBA	Sync.	GBA	Hop-BW	GBA	Hop-BS	GBA	BSP
78K( $\pm$ 23K)	74K( $\pm$ 25K)	0.7864	0.7864	300K	1,454	0.06 (2)	0.21 (11)	2.61 (12)
90K( $\pm$ 15K)	87K( $\pm$ 19K)	0.7864	0.7866	300K	898	0.04 (2)	0.15 (11)	1.92 (12)
99K( $\pm$ 12K)	98K( $\pm$ 12K)	0.7864	0.7865	300K	786	0.03 (2)	0.12 (9)	1.62 (10)

## 5.2 Performance of Training Modes

We first examine the performance of GBA. Figure 6(a-c) records the AUC tendencies after switching from synchronous to the other training modes over the three recommendation tasks. We mainly focus on the AUC at the first day and the last day, as well as the average AUC scores throughout the datasets. Although Hop-BW eliminates staleness, the ignorance of a large volume of data makes it perform the worst (also taken as evidence why we tend not to use local all-reduce in training recommender systems). The manipulation of global batch size contributes to the best performance on both sides of switching. Compared to the best baselines (i.e., Hop-BW), GBA improves AUC by at least 0.2% on average over the three datasets, which has the potential to increase by 1% revenue in the real-world business. Meanwhile, after switching from synchronous training, GBA obtains immediate good accuracy (AUC at the first day), while there are explicit re-convergence on the other training modes, as depicted in Figure 6(g).

Figure 6(d-f,h) illustrates the AUCs of these training modes after switching to synchronous training. We can see that GBA tends to obtain at least equal accuracy to the continuous synchronous training without switching. On the contrary, the models inherited from the other baselines require consuming more data to reach the desired accuracy of the synchronous training. The tendency of the AUC gaps between the synchronous training and the compared training modes reflects that the parameters trained by GBA are the most compatible with the synchronous training. It verifies that switching from GBA to synchronous training is also tuning-free.

We collect metrics of the training efficiency during the above experiments, and report their global QPS in Tab. 5.2. The results reveal that GBA performs similarly to the asynchronous training. Although Hop-BS works better than BSP and Hop-BW in accuracy, it struggles to deal with the slow workers. It indicates that when facing a resource shortage in the shared cluster, GBA can provide similar accuracy with synchronous training mode, while running as fast as the asynchronous training mode.

## 5.3 Fine-grained Analysis

We further probe into the performance of GBA. Here, we take the recommendation task on the Private dataset (the most complex model) as an example, switching from the synchronous mode to GBA.

We first analyze how the cluster status affects the performance of GBA. The experiments are repeated in the cluster during different periods of a day. We collect AUC, QPS, average gradient staleness on the dense parameters (for fair comparison among the baselines), and the number of excluded batches, as shown in Tab. 5.3. From the results, we can infer that GBA properly finds the balance between the staleness and the excluded data (as defined in Eqn. (1)), i.e., excluding fewer data compared to Hop-BW and suppressing the staleness to the same level of Hop-BS. GBA also shows strong robustness on the dynamic cluster status, obtaining stable performance on AUC.

We then examine the impact of the batch sizes in GBA. Figure 7 depicts the average AUC score and the global QPS when we modify the local batch size (the number of workers is thereby changed) and keep the global batch size unchanged. Considering the hardware limitation on worker and the communication overhead on PS, we vary the number of workers from 100 to 800. We can see a steady state of the AUC score (i.e., absolute difference less than  $10^{-4}$ ), while the training achieves



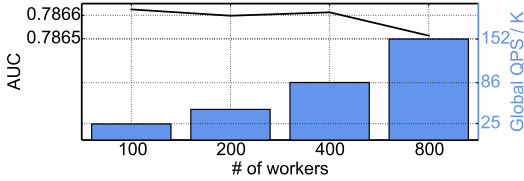


Figure 7: The average AUC on the 8-day test sets and the training efficiency via GBA, varying the number of workers while maintaining the global batch size.

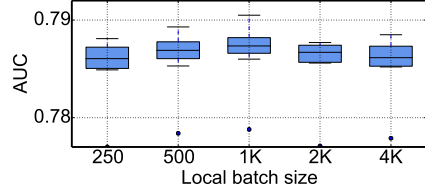


Figure 8: The range of AUC on the 8-day test sets via GBA of 400 workers, varying the local batch size.

a significant efficiency boost when using more workers. It can thereby be inferred that GBA has a good capability of scaling out. Besides, we fix the number of workers to 400 and change the local batch size for each worker, which means that the global batch size would differ. As shown in Fig. 8, the inconsistent global batch size with the synchronous training makes the training encounter lower AUC scores after switching. Although the larger global batch size may have the potential to achieve better accuracy (i.e., owing to the stable and accurate gradient), the experiment indicates the model would hardly reach its best accuracy without tuning. These results verify that using the same global batch size in GBA as in the synchronous training is necessary to get rid of tuning when switching the training mode.

## 6 Conclusion

A tuning-free switching approach is demanded to take full advantage of the synchronous and asynchronous training, which can improve the training efficiency in the shared cluster. We raise insights from the investigation over the production training workloads that the inconsistent batch size and the gradient staleness are two main reasons to fail the switching regarding the model accuracy. Then GBA training mode is proposed for asynchronously training recommendation models via aggregating gradients by the global batch size. GBA enables switching between synchronous training and asynchronous training of the continual learning tasks with the accuracy and efficiency guarantees. With GBA, users can freely switch the training modes according to the status of the shared training clusters, without tuning hyper-parameters. GBA is implemented through a token-control mechanism to ensure that the faster worker should contribute more gradients to the aggregation while the gradients from the straggling workers would be decayed. Evaluations of three representative continual training tasks of recommender systems reveal that GBA achieves similar accuracy with the synchronous training, while resembling the efficiency of the canonical asynchronous training. Currently, GBA requires the users to select the training mode according to their own judgment on the cluster status. In the future, we will attempt to make GBA be adaptive to the cluster status. The guidelines of automatic switching would be derived from more analyses upon the training trace logs. It could be formulated as an optimization problem under many control factors including but not limited to the overall QPS, training cost, and task scheduling with priority.

## References

- [1] B. Acun, M. Murphy, X. Wang, J. Nie, C.-J. Wu, and K. Hazelwood. Understanding training efficiency of deep learning recommendation models at scale. In *2021 IEEE International Symposium on High-Performance Computer Architecture (HPCA)*, pages 802–814. IEEE, 2021.
- [2] Y. Chen, J. Wang, Y. Lu, Y. Han, Z. Lv, X. Min, H. Cai, W. Zhang, H. Fan, C. Li, et al. Fangorn: adaptive execution framework for heterogeneous workloads on shared clusters. *Proceedings of the VLDB Endowment*, 14(12):2972–2985, 2021.
- [3] H.-T. Cheng, L. Koc, J. Harmsen, T. Shaked, T. Chandra, H. Aradhye, G. Anderson, G. Corrado, W. Chai, M. Ispir, et al. Wide & deep learning for recommender systems. In *Proceedings of the 1st workshop on deep learning for recommender systems*, pages 7–10, 2016.
- [4] D. community. Deeprec. <https://github.com/alibaba/DeepRec> 2022.5.11.

- [5] P. Covington, J. Adams, and E. Sargin. Deep neural networks for youtube recommendations. In *Proceedings of the 10th ACM conference on recommender systems*, pages 191–198, 2016.
- [6] S. Dutta, G. Joshi, S. Ghosh, P. Dube, and P. Nagpurkar. Slow and stale gradients can win the race: Error-runtime trade-offs in distributed SGD. In *International Conference on Artificial Intelligence and Statistics*, pages 803–812. PMLR, 2018.
- [7] S. Eliad, I. Hakimi, A. De Jagger, M. Silberstein, and A. Schuster. Fine-tuning giant neural networks on commodity hardware with automatic pipeline model parallelism. In *2021 USENIX Annual Technical Conference (USENIX ATC 21)*, pages 381–396, 2021.
- [8] A. Group. Ad display/click data on taobao.com. <https://tianchi.aliyun.com/dataset/dataDetail?dataId=56&lang=en-us> under CC BY-NC-SA 4.0, visited on 2022.5.11.
- [9] Y. Guo, M. Liu, T. Yang, and T. Rosing. Improved schemes for episodic memory-based lifelong learning. *Advances in Neural Information Processing Systems*, 33:1023–1035, 2020.
- [10] F. He, T. Liu, and D. Tao. Control batch size and learning rate to generalize well: Theoretical and empirical evidence. *Advances in Neural Information Processing Systems*, 32, 2019.
- [11] Q. Ho, J. Cipar, H. Cui, S. Lee, J. K. Kim, P. B. Gibbons, G. A. Gibson, G. Ganger, and E. P. Xing. More effective distributed ml via a stale synchronous parallel parameter server. *Advances in neural information processing systems*, 26, 2013.
- [12] J. Hron, K. Krauth, M. Jordan, and N. Kilbertus. On component interactions in two-stage recommender systems. *Advances in Neural Information Processing Systems*, 34, 2021.
- [13] C. Inc. Criteo 1tb click logs dataset. <https://ailab.criteo.com/download-criteo-1tb-click-logs-dataset/> visited on 2022.5.11, .
- [14] C. Inc. Kaggle display advertising challenge dataset. <http://labs.criteo.com/2014/02/kaggle-display-advertising-challenge-dataset/> visited on 2020.1.10, .
- [15] Y. Jiang, Y. Zhu, C. Lan, B. Yi, Y. Cui, and C. Guo. A unified architecture for accelerating distributed {DNN} training in heterogeneous {GPU/CPU} clusters. In *14th USENIX Symposium on Operating Systems Design and Implementation (OSDI 20)*, pages 463–479, 2020.
- [16] S. Kim, G.-I. Yu, H. Park, S. Cho, E. Jeong, H. Ha, S. Lee, J. S. Jeong, and B.-G. Chun. Parallax: Sparsity-aware data parallel training of deep neural networks. In *Proceedings of the Fourteenth EuroSys Conference 2019*, pages 1–15, 2019.
- [17] A. Kumar, A. Beutel, Q. Ho, and E. Xing. Fugue: Slow-worker-agnostic distributed learning for big models on big data. In *Artificial Intelligence and Statistics*, pages 531–539. PMLR, 2014.
- [18] L. Li, K. Jamieson, A. Rostamizadeh, E. Gonina, J. Ben-Tzur, M. Hardt, B. Recht, and A. Talwalkar. A system for massively parallel hyperparameter tuning. *Proceedings of Machine Learning and Systems*, 2:230–246, 2020.
- [19] M. Li, D. G. Andersen, J. W. Park, A. J. Smola, A. Ahmed, V. Josifovski, J. Long, E. J. Shekita, and B.-Y. Su. Scaling distributed machine learning with the parameter server. In *11th USENIX Symposium on Operating Systems Design and Implementation (OSDI 14)*, pages 583–598, 2014.
- [20] S. Li, O. Mangoubi, L. Xu, and T. Guo. Sync-switch: Hybrid parameter synchronization for distributed deep learning. In *2021 IEEE 41st International Conference on Distributed Computing Systems (ICDCS)*, pages 528–538. IEEE, 2021.
- [21] J. Lian, X. Zhou, F. Zhang, Z. Chen, X. Xie, and G. Sun. xdeepfm: Combining explicit and implicit feature interactions for recommender systems. In *Proceedings of the 24th ACM SIGKDD International Conference on Knowledge Discovery & Data Mining*, pages 1754–1763, 2018.
- [22] Q. Luo, J. Lin, Y. Zhuo, and X. Qian. Hop: Heterogeneity-aware decentralized training. In *Proceedings of the Twenty-Fourth International Conference on Architectural Support for Programming Languages and Operating Systems*, pages 893–907, 2019.

- [23] Q. Luo, J. He, Y. Zhuo, and X. Qian. Prague: High-performance heterogeneity-aware asynchronous decentralized training. In *Proceedings of the Twenty-Fifth International Conference on Architectural Support for Programming Languages and Operating Systems*, pages 401–416, 2020.
- [24] G. Nadiradze, A. Sabour, P. Davies, S. Li, and D. Alistarh. Asynchronous decentralized sgd with quantized and local updates. *Advances in Neural Information Processing Systems*, 34, 2021.
- [25] J. Wu, W. Hu, H. Xiong, J. Huan, V. Braverman, and Z. Zhu. On the noisy gradient descent that generalizes as sgd. In *International Conference on Machine Learning*, pages 10367–10376. PMLR, 2020.
- [26] B. Ying, K. Yuan, Y. Chen, H. Hu, P. Pan, and W. Yin. Exponential graph is provably efficient for decentralized deep training. *Advances in Neural Information Processing Systems*, 34, 2021.
- [27] Y. You, J. Li, S. Reddi, J. Hseu, S. Kumar, S. Bhojanapalli, X. Song, J. Demmel, K. Keutzer, and C.-J. Hsieh. Large batch optimization for deep learning: Training bert in 76 minutes. In *ICLR*, 2020.
- [28] H. Yu and R. Jin. On the computation and communication complexity of parallel sgd with dynamic batch sizes for stochastic non-convex optimization. In *International Conference on Machine Learning*, pages 7174–7183. PMLR, 2019.
- [29] Y. Zhang, L. Chen, S. Yang, M. Yuan, H. Yi, J. Zhang, J. Wang, J. Dong, Y. Xu, Y. Song, et al. Picasso: Unleashing the potential of gpu-centric training for wide-and-deep recommender systems. In *2022 IEEE International Conference on Data Engineering (ICDE)*, 2022.
- [30] S. Zheng, Q. Meng, T. Wang, W. Chen, N. Yu, Z.-M. Ma, and T.-Y. Liu. Asynchronous stochastic gradient descent with delay compensation. In *International Conference on Machine Learning*, pages 4120–4129. PMLR, 2017.
- [31] G. Zhou, X. Zhu, C. Song, Y. Fan, H. Zhu, X. Ma, Y. Yan, J. Jin, H. Li, and K. Gai. Deep interest network for click-through rate prediction. In *Proceedings of the 24th ACM SIGKDD international conference on knowledge discovery & data mining*, pages 1059–1068, 2018.
- [32] G. Zhou, N. Mou, Y. Fan, Q. Pi, W. Bian, C. Zhou, X. Zhu, and K. Gai. Deep interest evolution network for click-through rate prediction. In *Proceedings of the AAAI conference on artificial intelligence*, volume 33, pages 5941–5948, 2019.
- [33] Y. Zhou, Y. Yu, W. Dai, Y. Liang, and E. Xing. On convergence of model parallel proximal gradient algorithm for stale synchronous parallel system. In *Artificial Intelligence and Statistics*, pages 713–722. PMLR, 2016.

## Appendix

### A Proof of Equation (4)

**Assumption.** Throughout the paper, we make the following assumptions:

1.  $F(w)$  is an L-smooth function, i.e.,  $F(w_1) \leq F(w_2) + (w_1 - w_2)^T \nabla F(w_2) + \frac{L}{2} \|w_1 - w_2\|_2^2$ ;
2.  $F(w)$  is strongly convex with parameter  $c$ , i.e.,  $2c(F(w) - F^*) \leq \|\nabla F(w)\|_2^2$ ;
3. The stochastic gradient  $g(w_{\tau(m,k)})$  is an unbiased estimate of the true gradient, i.e.,

$$E(g(w_{\tau(m,k)})) = E(\nabla F(w_{\tau(m,k)}));$$

4. The variance of the stochastic gradient  $g(w_{\tau(m,k)})$  in the asynchronous training is bounded as

$$E\left(\|g(w_{\tau(m,k)}) - \nabla F(w_{\tau(m,k)})\|_2^2\right) \leq \frac{\sigma^2}{B_a} + \frac{\Theta}{B_a} E(\|\nabla F(w_{\tau(m,k)})\|_2^2),$$

and in the synchronous training is bounded as

$$E\left(\|g(w_{\tau(m,k)}) - \nabla F(w_{\tau(m,k)})\|_2^2\right) \leq \frac{\sigma^2}{B_s} + \frac{\Theta}{B_s} E(\|\nabla F(w_{\tau(m,k)})\|_2^2).$$

**Theorem 1.** Based on the above Assumption and  $\eta \leq \frac{1}{2L(\frac{\Theta}{MB_a} + 1)}$ , also suppose that for some  $\gamma \leq 1$ ,

$$E\left(\|\nabla F(w_k) - \nabla F(w_{\tau(m,k)})\|_2^2\right) \leq \gamma E(\|\nabla F(w_k)\|_2^2),$$

thus the expectation of error after  $k + 1$  steps of gradient updates **in the asynchronous training** is deduced by

$$E(F(w_{k+1}) - F^*) \leq \frac{\eta L \sigma^2}{2c\gamma' M B_a} + (1 - \eta\gamma'c)^{k+1} \left( E(F(w_0) - F^*) - \frac{\eta L \sigma^2}{2c\gamma' M B_a} \right),$$

where  $\gamma' = 1 - \gamma + \frac{p_0}{2}$ ,  $p_0$  is a lower bound on the conditional probability that the token equals to the global step, i.e.,  $\tau(m, k) = k$ .

**Corollary 1.** To characterize the strong sparsity in the recommendation models, we suppose that for some  $\gamma \leq 1$ ,

$$\zeta E(\|\nabla F(w_k) - \nabla F(w_{\tau(m,k)})\|_2^2) \leq \gamma E(\|\nabla F(w_k)\|_2^2),$$

$$\gamma = \begin{cases} \gamma, & \varsigma = 1, \\ \zeta\gamma, & \varsigma \neq 1, \end{cases} \quad (5)$$

thus the expectation of error after  $k + 1$  steps of gradient updates **in the asynchronous training** is

$$E(F(w_{k+1}) - F^*) \leq \frac{\eta L \sigma^2}{2c\rho M B_a} + (1 - \eta\rho c)^{k+1} \left( E(F(w_0) - F^*) - \frac{\eta L \sigma^2}{2c\rho M B_a} \right),$$

where  $\rho = 1 - p_1\gamma - (1 - p_1)\zeta\gamma + \frac{p_0}{2}$ ,  $\varsigma = \mathbb{I}_{dense}(parameter)$ ,  $\mathbb{I}_A(x)$  is the indicator function of whether  $x$  belongs to  $A$ ,  $p_1 = P(\varsigma = 1)$ .

It is worth noting that we have  $\rho > 0$  and  $\rho > \gamma'$  owing to  $\zeta\gamma < \gamma \leq 1$ . Since  $\frac{2+p_0-2\zeta\gamma}{2(\gamma-\zeta\gamma)} > 1$ ,  $P(\varsigma = 1) < \frac{2+p_0-2\zeta\gamma}{2(\gamma-\zeta\gamma)}$ . The model GBA achieves a better performance in terms of dense and sparse parameters, like the error floor  $\frac{\eta L \sigma^2}{2c\rho M B_a}$  is smaller than  $\frac{\eta L \sigma^2}{2c\gamma' M B_a}$  mentioned in Theorem 1, and the convergence speed is more quickly. Clearly, the value of  $p_1$  is differ for various distributions and accordingly the values of  $\frac{\eta L \sigma^2}{2c\rho M B_a}$  and  $1 - \eta\rho c$  are different.

**Theorem 2.** Based on the above Assumption and  $\eta \leq \frac{1}{2L(\frac{\Theta}{N_s B_s} + 1)}$ , the expectation of error after  $k + 1$  steps of gradient updates **in the synchronous training** is deduced by

$$E(F(w_{k+1}) - F^*) \leq \frac{\eta L \sigma^2}{2cN_s B_s} + (1 - \eta c)^{k+1} \left( E(F(w_0) - F^*) - \frac{\eta L \sigma^2}{2cN_s B_s} \right).$$

To provide the proofs of Theorem 1, Corollary 1, and Theorem 2, we first prove the following lemmas.

**Lemma 1.** Let  $g(w_{\tau(i,k)})$  denote the  $i$ -th gradient of  $k$ -th global step, and assume its expectation  $E(g(w_{\tau(i,k)})) = E(\nabla F(w_{\tau(i,k)}))$ . Then

$$\begin{aligned} & E\left(\|g(w_{\tau(i,k)}) - \nabla F(w_k)\|_2^2\right) \\ &= E(\|g(w_{\tau(i,k)})\|_2^2) - E(\|\nabla F(w_{\tau(i,k)})\|_2^2) + E\left(\|\nabla F(w_{\tau(i,k)}) - \nabla F(w_k)\|_2^2\right). \end{aligned}$$

*proof of Lemma 1.*

$$\begin{aligned} & E\left(\|g(w_{\tau(i,k)}) - \nabla F(w_k)\|_2^2\right) \\ &= E\left(\|g(w_{\tau(i,k)}) - \nabla F(w_{\tau(i,k)}) + \nabla F(w_{\tau(i,k)}) - \nabla F(w_k)\|_2^2\right) \\ &= E\left(\|g(w_{\tau(i,k)}) - \nabla F(w_{\tau(i,k)})\|_2^2\right) + E\left(\|\nabla F(w_{\tau(i,k)}) - \nabla F(w_k)\|_2^2\right) \\ &\quad + 2E\left(\left\langle g(w_{\tau(i,k)}) - \nabla F(w_{\tau(i,k)}), \nabla F(w_{\tau(i,k)}) - \nabla F(w_k) \right\rangle\right). \end{aligned} \tag{6}$$

Since  $E(g(w_{\tau(i,k)})) = E(\nabla F(w_{\tau(i,k)}))$ ,

$$E\left(\left\langle g(w_{\tau(i,k)}) - \nabla F(w_{\tau(i,k)}), \nabla F(w_{\tau(i,k)}) - \nabla F(w_k) \right\rangle\right) = 0.$$

Returning to (6), we have

$$\begin{aligned} & E\left(\|g(w_{\tau(i,k)}) - \nabla F(w_k)\|_2^2\right) \\ &= E\left(\|g(w_{\tau(i,k)}) - \nabla F(w_{\tau(i,k)})\|_2^2\right) + E\left(\|\nabla F(w_{\tau(i,k)}) - \nabla F(w_k)\|_2^2\right) \\ &= E(\|g(w_{\tau(i,k)})\|_2^2) + E(\|\nabla F(w_{\tau(i,k)})\|_2^2) - 2E\left(\langle g(w_{\tau(i,k)}), \nabla F(w_{\tau(i,k)}) \rangle\right) \\ &\quad + E\left(\|\nabla F(w_{\tau(i,k)}) - \nabla F(w_k)\|_2^2\right) \\ &= E(\|g(w_{\tau(i,k)})\|_2^2) - E(\|\nabla F(w_{\tau(i,k)})\|_2^2) + E\left(\|\nabla F(w_{\tau(i,k)}) - \nabla F(w_k)\|_2^2\right). \end{aligned} \tag{7}$$

□

**Lemma 2.** Let  $v_k = \frac{1}{M} \sum_{i=1}^M g(w_{\tau(i,k)})$ , and suppose the variance of  $g(w_{\tau(i,k)})$  is bounded as

$$E\left(\|g(w_{\tau(i,k)}) - \nabla F(w_{\tau(i,k)})\|_2^2\right) \leq \frac{\sigma^2}{B_a} + \frac{\Theta}{B_a} \|\nabla F(w_{\tau(i,k)})\|_2^2.$$

Then the sum of  $g(w_{\tau(i,k)})$  is bounded as follows

$$E(\|v_k\|_2^2) \leq \frac{\sigma^2}{MB_a} + \sum_{i=1}^M \frac{\Theta}{M^2 B_a} E(\|\nabla F(w_{\tau(i,k)})\|_2^2) + \frac{1}{M} \sum_{i=1}^M E(\|\nabla F(w_{\tau(i,k)})\|_2^2).$$

*proof of Lemma 2.*

$$\begin{aligned} E(\|v_k\|_2^2) &= E\left(\left\|\frac{1}{M} \sum_{i=1}^M g(w_{\tau(i,k)})\right\|_2^2\right) = \frac{1}{M^2} E\left(\left\|\sum_{i=1}^M g(w_{\tau(i,k)})\right\|_2^2\right) \\ &= \frac{1}{M^2} E\left(\left\|\sum_{i=1}^M (g(w_{\tau(i,k)}) - \nabla F(w_{\tau(i,k)})) + \sum_{i=1}^M \nabla F(w_{\tau(i,k)})\right\|_2^2\right) \\ &= \frac{1}{M^2} E\left(\left\|\sum_{i=1}^M (g(w_{\tau(i,k)}) - \nabla F(w_{\tau(i,k)}))\right\|_2^2\right) + \frac{1}{M^2} E\left(\left\|\sum_{i=1}^M \nabla F(w_{\tau(i,k)})\right\|_2^2\right) \\ &\quad + \frac{2}{M^2} E\left(\left\langle \sum_{i=1}^M (g(w_{\tau(i,k)}) - \nabla F(w_{\tau(i,k)})), \sum_{i=1}^M \nabla F(w_{\tau(i,k)}) \right\rangle\right) \end{aligned} \tag{8}$$

Owing to  $E(g(w_{\tau(i,k)})) = E(\nabla F(w_{\tau(i,k)}))$ ,

$$\begin{aligned}
E(\|v_k\|_2^2) &= \frac{1}{M^2} E\left(\left\|\sum_{i=1}^M (g(w_{\tau(i,k)}) - \nabla F(w_{\tau(i,k)}))\right\|_2^2\right) + \frac{1}{M^2} E\left(\left\|\sum_{i=1}^M \nabla F(w_{\tau(i,k)})\right\|_2^2\right) \\
&= \frac{1}{M^2} \sum_{i=1}^M E\left(\|g(w_{\tau(i,k)}) - \nabla F(w_{\tau(i,k)})\|_2^2\right) + \frac{1}{M^2} E\left(\left\|\sum_{i=1}^M \nabla F(w_{\tau(i,k)})\right\|_2^2\right) \\
&\quad + \frac{2}{M^2} \sum_{i=1}^{M-1} \sum_{j=i+1}^M E\left(\langle g(w_{\tau(i,k)}) - \nabla F(w_{\tau(i,k)}), g(w_{\tau(j,k)}) - \nabla F(w_{\tau(j,k)}) \rangle\right) \quad (9) \\
&= \frac{1}{M^2} \sum_{i=1}^M E\left(\|g(w_{\tau(i,k)}) - \nabla F(w_{\tau(i,k)})\|_2^2\right) + \frac{1}{M^2} E\left(\left\|\sum_{i=1}^M \nabla F(w_{\tau(i,k)})\right\|_2^2\right) \\
&\leq \frac{\sigma^2}{MB_a} + \sum_{i=1}^M \frac{\Theta}{M^2 B_a} E(\|\nabla F(w_{\tau(i,k)})\|_2^2) + \frac{1}{M^2} E\left(\left\|\sum_{i=1}^M \nabla F(w_{\tau(i,k)})\right\|_2^2\right).
\end{aligned}$$

The second term in (9) could be obtained by

$$\begin{aligned}
&E\left(\left\|\sum_{i=1}^M \nabla F(w_{\tau(i,k)})\right\|_2^2\right) \\
&= \sum_{i=1}^M E(\|\nabla F(w_{\tau(i,k)})\|_2^2) + \sum_{i=1}^{M-1} \sum_{j=i+1}^M 2E(\langle \nabla F(w_{\tau(i,k)}), \nabla F(w_{\tau(j,k)}) \rangle) \\
&\stackrel{(a)}{\leq} \sum_{i=1}^M E(\|\nabla F(w_{\tau(i,k)})\|_2^2) + \sum_{i=1}^{M-1} \sum_{j=i+1}^M E\left(\|\nabla F(w_{\tau(i,k)})\|_2^2 + \|\nabla F(w_{\tau(j,k)})\|_2^2\right) \quad (10) \\
&= \sum_{i=1}^M E(\|\nabla F(w_{\tau(i,k)})\|_2^2) + \sum_{i=1}^M (M-1)E(\|\nabla F(w_{\tau(i,k)})\|_2^2) \\
&= \sum_{i=1}^M ME(\|\nabla F(w_{\tau(i,k)})\|_2^2).
\end{aligned}$$

Here step (a) follows from  $2\langle x, y \rangle \leq \|x\|_2^2 + \|y\|_2^2$ .

Based on (9) and (10), we have

$$E(\|v_k\|_2^2) \leq \frac{\sigma^2}{MB_a} + \sum_{i=1}^M \frac{\Theta}{M^2 B_a} E(\|\nabla F(w_{\tau(i,k)})\|_2^2) + \frac{1}{M} \sum_{i=1}^M E(\|\nabla F(w_{\tau(i,k)})\|_2^2).$$

□

**Lemma 3.** Suppose  $p_0$  is a lower bound on the conditional probability that the token equals to the global step, i.e.,  $\tau(i, k) = k$ , thus

$$E(\|\nabla F(w_{\tau(i,k)})\|_2^2) \geq p_0 E(\|\nabla F(w_k)\|_2^2).$$

*proof of Lemma 3.*

$$\begin{aligned}
E(\|\nabla F(w_{\tau(i,k)})\|_2^2) &= p_0 E\left(\|\nabla F(w_{\tau(i,k)})\|_2^2 \mid \tau(i, k) = k\right) \\
&\quad + (1 - p_0) E\left(\|\nabla F(w_{\tau(i,k)})\|_2^2 \mid \tau(i, k) \neq k\right) \quad (11) \\
&\geq p_0 E(\|\nabla F(w_k)\|_2^2).
\end{aligned}$$

□

Next, we will provide the proofs of Theorem 1, Corollary 1, and Theorem 2.

*proof of Theorem 1.* Let  $w_{k+1} = w_k - \eta v_k$ ,  $v_k = \frac{1}{M} \sum_{i=1}^M g(w_{\tau(i,k)})$ , we have

$$\begin{aligned} F(w_{k+1}) &\leq F(w_k) + (w_{k+1} - w_k)^T \nabla F(w_k) + \frac{L}{2} \|w_{k+1} - w_k\|_2^2 \\ &\leq F(w_k) + \langle -\eta v_k, \nabla F(w_k) \rangle + \frac{L}{2} \eta^2 \|v_k\|_2^2 \\ &= F(w_k) - \frac{\eta}{M} \sum_{i=1}^M \langle g(w_{\tau(i,k)}), \nabla F(w_k) \rangle + \frac{L}{2} \eta^2 \|v_k\|_2^2. \end{aligned} \quad (12)$$

Owing to  $2\langle x, y \rangle = \|x\|_2^2 + \|y\|_2^2 - \|x - y\|_2^2$ , (12) is shown as follows,

$$\begin{aligned} F(w_{k+1}) &\leq F(w_k) - \frac{\eta}{M} \sum_{i=1}^M \left( \frac{1}{2} \|g(w_{\tau(i,k)})\|_2^2 + \frac{1}{2} \|\nabla F(w_k)\|_2^2 - \frac{1}{2} \|g(w_{\tau(i,k)}) - \nabla F(w_k)\|_2^2 \right) + \frac{L}{2} \eta^2 \|v_k\|_2^2 \\ &= F(w_k) - \frac{\eta}{2} \|\nabla F(w_k)\|_2^2 - \frac{\eta}{2M} \sum_{i=1}^M \|g(w_{\tau(i,k)})\|_2^2 + \frac{\eta}{2M} \sum_{i=1}^M \|g(w_{\tau(i,k)}) - \nabla F(w_k)\|_2^2 + \frac{L}{2} \eta^2 \|v_k\|_2^2. \end{aligned} \quad (13)$$

Taking expectation,

$$\begin{aligned} E(F(w_{k+1})) &\leq E(F(w_k)) - \frac{\eta}{2} E(\|\nabla F(w_k)\|_2^2) - \frac{\eta}{2M} \sum_{i=1}^M E(\|g(w_{\tau(i,k)})\|_2^2) \\ &\quad + \frac{\eta}{2M} \sum_{i=1}^M E(\|g(w_{\tau(i,k)}) - \nabla F(w_k)\|_2^2) + \frac{L}{2} \eta^2 E(\|v_k\|_2^2) \\ &\stackrel{(a)}{=} E(F(w_k)) - \frac{\eta}{2} E(\|\nabla F(w_k)\|_2^2) - \frac{\eta}{2M} \sum_{i=1}^M E(\|g(w_{\tau(i,k)})\|_2^2) + \frac{\eta}{2M} \sum_{i=1}^M E(\|g(w_{\tau(i,k)})\|_2^2) \\ &\quad - \frac{\eta}{2M} \sum_{i=1}^M E(\|\nabla F(w_{\tau(i,k)})\|_2^2) + \frac{\eta}{2M} \sum_{i=1}^M E(\|\nabla F(w_{\tau(i,k)}) - \nabla F(w_k)\|_2^2) + \frac{L}{2} \eta^2 E(\|v_k\|_2^2) \\ &\stackrel{(b)}{\leq} E(F(w_k)) - \frac{\eta}{2} E(\|\nabla F(w_k)\|_2^2) - \frac{\eta}{2M} \sum_{i=1}^M E(\|\nabla F(w_{\tau(i,k)})\|_2^2) \\ &\quad + \frac{\eta}{2} \gamma E(\|\nabla F(w_k)\|_2^2) + \frac{L}{2} \eta^2 E(\|v_k\|_2^2) \\ &= E(F(w_k)) - \frac{\eta}{2} (1 - \gamma) E(\|\nabla F(w_k)\|_2^2) - \frac{\eta}{2M} \sum_{i=1}^M E(\|\nabla F(w_{\tau(i,k)})\|_2^2) + \frac{L}{2} \eta^2 E(\|v_k\|_2^2) \\ &\stackrel{(c)}{\leq} E(F(w_k)) - \frac{\eta}{2} (1 - \gamma) E(\|\nabla F(w_k)\|_2^2) - \frac{\eta}{2M} \sum_{i=1}^M E(\|\nabla F(w_{\tau(i,k)})\|_2^2) \\ &\quad + \frac{L}{2} \eta^2 \left( \frac{\sigma^2}{MB_a} + \sum_{i=1}^M \frac{\Theta}{M^2 B_a} E(\|\nabla F(w_{\tau(i,k)})\|_2^2) + \frac{1}{M} \sum_{i=1}^M E(\|\nabla F(w_{\tau(i,k)})\|_2^2) \right) \\ &= E(F(w_k)) - \frac{\eta}{2} (1 - \gamma) E(\|\nabla F(w_k)\|_2^2) + \frac{L\eta^2 \sigma^2}{2MB_a} \\ &\quad - \frac{\eta}{2M} \sum_{i=1}^M \left( 1 - \frac{L\eta\Theta}{MB_a} - L\eta \right) E(\|\nabla F(w_{\tau(i,k)})\|_2^2). \end{aligned} \quad (14)$$

Here step (a) follows from Lemma 1, step (b) follow from  $E(\|\nabla F(w_k) - \nabla F(w_{\tau(m,k)})\|_2^2) \leq \gamma E(\|\nabla F(w_k)\|_2^2)$ , and step (c) follows from Lemma 2.

Since  $\eta \leq \frac{1}{2L(\frac{\sigma}{MB_a} + 1)}$ , (14) could be obtained by

$$\begin{aligned}
E(F(w_{k+1})) &\leq E(F(w_k)) - \frac{\eta}{2}(1 - \gamma)E(\|\nabla F(w_k)\|_2^2) + \frac{L\eta^2\sigma^2}{2MB_a} - \frac{\eta}{4M} \sum_{i=1}^M E(\|\nabla F(w_{\tau(i,k)})\|_2^2) \\
&\stackrel{(d)}{\leq} E(F(w_k)) - \frac{\eta}{2}(1 - \gamma)E(\|\nabla F(w_k)\|_2^2) + \frac{L\eta^2\sigma^2}{2MB_a} - \frac{\eta}{4}p_0E(\|\nabla F(w_k)\|_2^2) \\
&\stackrel{(e)}{\leq} E(F(w_k)) - \eta c(1 - \gamma)E(F(w_k) - F^*) - \frac{\eta c p_0}{2}E(F(w_k) - F^*) + \frac{L\eta^2\sigma^2}{2MB_a} \\
&= E(F(w_k)) - \eta c \gamma' E(F(w_k) - F^*) + \frac{L\eta^2\sigma^2}{2MB_a},
\end{aligned} \tag{15}$$

where  $\gamma' = 1 - \gamma + \frac{p_0}{2}$ . Here step (d) follows from Lemma 3, step (e) follows from  $F(w)$  is strongly convex with parameter  $c$ .

Therefore,

$$E(F(w_{k+1}) - F^*) \leq \frac{\eta L \sigma^2}{2c \gamma' M B_a} + (1 - \eta \gamma' c)^{k+1} \left( E(F(w_0) - F^*) - \frac{\eta L \sigma^2}{2c \gamma' M B_a} \right).$$

□

*proof of Corollary 1.* Based on  $\zeta E(\|\nabla F(w_k) - \nabla F(w_{\tau(m,k)})\|_2^2) \leq \gamma E(\|\nabla F(w_k)\|_2^2)$ , the step (b) of (14) should be written as follows,

$$\begin{aligned}
E(F(w_{k+1})) &\leq E(F(w_k)) - \frac{\eta}{2}E(\|\nabla F(w_k)\|_2^2) - \frac{\eta}{2M} \sum_{i=1}^M E(\|\nabla F(w_{\tau(i,k)})\|_2^2) \\
&\quad + \frac{L\eta^2}{2}E(\|v_k\|_2^2) + \frac{\eta}{2M} \sum_{i=1}^M E\left(\|\nabla F(w_{\tau(i,k)}) - \nabla F(w_k) \mid \varsigma = 1\|_2^2\right) \\
&\quad + \frac{\eta}{2M} \sum_{i=1}^M E\left(\|\nabla F(w_{\tau(i,k)}) - \nabla F(w_k) \mid \varsigma \neq 1\|_2^2\right) \\
&\leq E(F(w_k)) - \frac{\eta}{2}E(\|\nabla F(w_k)\|_2^2) - \frac{\eta}{2M} \sum_{i=1}^M E(\|\nabla F(w_{\tau(i,k)})\|_2^2) \\
&\quad + \frac{L\eta^2}{2}E(\|v_k\|_2^2) + \frac{\eta \gamma p_1}{2M} \sum_{i=1}^M E(\|\nabla F(w_k)\|_2^2) + \frac{\eta \zeta \gamma (1 - p_1)}{2M} \sum_{i=1}^M E(\|\nabla F(w_k)\|_2^2) \\
&= E(F(w_k)) - \frac{\eta}{2} \left( 1 - p_1 \gamma - (1 - p_1) \zeta \gamma \right) E(\|\nabla F(w_k)\|_2^2) \\
&\quad - \frac{\eta}{2M} \sum_{i=1}^M E(\|\nabla F(w_{\tau(i,k)})\|_2^2) + \frac{L\eta^2}{2}E(\|v_k\|_2^2) \\
&\leq E(F(w_k)) - \frac{\eta}{2} \left( 1 - p_1 \gamma - (1 - p_1) \zeta \gamma \right) E(\|\nabla F(w_k)\|_2^2) + \frac{L\eta^2\sigma^2}{2MB_a} \\
&\quad - \frac{\eta}{4M} \sum_{i=1}^M E(\|\nabla F(w_{\tau(i,k)})\|_2^2) \\
&\leq E(F(w_k)) - \frac{\eta}{2} \left( 1 - p_1 \gamma - (1 - p_1) \zeta \gamma + \frac{p_0}{2} \right) E(\|\nabla F(w_k)\|_2^2) + \frac{L\eta^2\sigma^2}{2MB_a} \\
&\leq E(F(w_k)) - \eta c \rho E(F(w_k) - F^*) + \frac{L\eta^2\sigma^2}{2MB_a}
\end{aligned} \tag{16}$$

where  $\rho = 1 - p_1 \gamma - (1 - p_1) \zeta \gamma + \frac{p_0}{2}$ ,  $p_1 = P(\varsigma = 1)$ . Therefore,

$$E(F(w_{k+1}) - F^*) \leq \frac{\eta L \sigma^2}{2c \rho M B_a} + (1 - \eta \rho c)^{k+1} \left( E(F(w_0) - F^*) - \frac{\eta L \sigma^2}{2c \rho M B_a} \right).$$



□

*proof of Theorem 2.* Let  $w_{k+1} = w_k - \eta v_k$ ,  $v_k = \frac{1}{N_s} \sum_{i=1}^{N_s} g(w_{\tau(i,k)})$ , we have

$$\begin{aligned}
F(w_{k+1}) &\leq F(w_k) + (w_{k+1} - w_k)^T \nabla F(w_k) + \frac{L}{2} \|w_{k+1} - w_k\|_2^2 \\
&= F(w_k) + \langle -\eta v_k, \nabla F(w_k) \rangle + \frac{L}{2} \eta^2 \|v_k\|_2^2 \\
&= F(w_k) - \frac{\eta}{N_s} \sum_{i=1}^{N_s} \langle g(w_{\tau(i,k)}), \nabla F(w_k) \rangle + \frac{L}{2} \eta^2 \|v_k\|_2^2 \\
&= F(w_k) - \frac{\eta}{N_s} \sum_{i=1}^{N_s} \left( \frac{1}{2} \|g(w_{\tau(i,k)})\|_2^2 + \frac{1}{2} \|\nabla F(w_k)\|_2^2 - \frac{1}{2} \|g(w_{\tau(i,k)}) - \nabla F(w_k)\|_2^2 \right) + \frac{L}{2} \eta^2 \|v_k\|_2^2 \\
&= F(w_k) - \frac{\eta}{2} \|\nabla F(w_k)\|_2^2 - \frac{\eta}{2N_s} \sum_{i=1}^{N_s} \|g(w_{\tau(i,k)})\|_2^2 + \frac{\eta}{2N_s} \sum_{i=1}^{N_s} \|g(w_{\tau(i,k)}) - \nabla F(w_k)\|_2^2 + \frac{L}{2} \eta^2 \|v_k\|_2^2.
\end{aligned} \tag{17}$$

Taking expectation,

$$\begin{aligned}
E(F(w_{k+1})) &\leq E(F(w_k)) - \frac{\eta}{2} E(\|\nabla F(w_k)\|_2^2) - \frac{\eta}{2N_s} \sum_{i=1}^{N_s} E(\|g(w_{\tau(i,k)})\|_2^2) + \frac{L}{2} \eta^2 E(\|v_k\|_2^2) \\
&\quad + \frac{\eta}{2N_s} \sum_{i=1}^{N_s} E(\|g(w_{\tau(i,k)}) - \nabla F(w_k)\|_2^2).
\end{aligned} \tag{18}$$

The last term in (18) could be obtained on the basis of  $E(g(w_{\tau(i,k)})) = E(\nabla F(w_k))$ ,

$$\begin{aligned}
&E(\|g(w_{\tau(i,k)}) - \nabla F(w_k)\|_2^2) \\
&= E(\|g(w_{\tau(i,k)})\|_2^2) + E(\|\nabla F(w_k)\|_2^2) - 2E(\langle g(w_{\tau(i,k)}), \nabla F(w_k) \rangle) \\
&= E(\|g(w_{\tau(i,k)})\|_2^2) - E(\|\nabla F(w_k)\|_2^2).
\end{aligned} \tag{19}$$

Returning to (18), we have

$$\begin{aligned}
E(F(w_{k+1})) &\leq E(F(w_k)) - \frac{\eta}{2} E(\|\nabla F(w_k)\|_2^2) - \frac{\eta}{2N_s} \sum_{i=1}^{N_s} E(\|g(w_{\tau(i,k)})\|_2^2) + \frac{L}{2} \eta^2 E(\|v_k\|_2^2) \\
&\quad + \frac{\eta}{2N_s} \sum_{i=1}^{N_s} E(\|g(w_{\tau(i,k)})\|_2^2) - \frac{\eta}{2N_s} \sum_{i=1}^{N_s} E(\|\nabla F(w_k)\|_2^2).
\end{aligned} \tag{20}$$

Similar to Lemma 2,

$$\begin{aligned}
E(\|v_k\|_2^2) &= E\left(\left\|\frac{1}{N_s} \sum_{i=1}^{N_s} g(w_{\tau(i,k)})\right\|_2^2\right) \\
&= \frac{1}{N_s^2} E\left(\left\|\sum_{i=1}^{N_s} (g(w_{\tau(i,k)}) - \nabla F(w_k))\right\|_2^2\right) + \frac{1}{N_s^2} E\left(\left\|\sum_{i=1}^{N_s} \nabla F(w_k)\right\|_2^2\right) \\
&= \frac{1}{N_s^2} \sum_{i=1}^{N_s} E(\|g(w_{\tau(i,k)}) - \nabla F(w_k)\|_2^2) + E(\|\nabla F(w_k)\|_2^2) \\
&\leq \frac{\sigma^2}{N_s B_s} + \left(\frac{\Theta}{N_s B_s} + 1\right) E(\|\nabla F(w_k)\|_2^2).
\end{aligned} \tag{21}$$

Based on (20) and (21), we obtain

$$\begin{aligned}
E(F(w_{k+1})) &\leq E(F(w_k)) - \eta E(\|\nabla F(w_k)\|_2^2) + \frac{L\eta^2\sigma^2}{2N_s B_s} + \frac{L\eta^2}{2} \left( \frac{\Theta}{N_s B_s} + 1 \right) E(\|\nabla F(w_k)\|_2^2) \\
&= E(F(w_k)) - \eta \left( 1 - \frac{L\eta\Theta}{2N_s B_s} - \frac{L\eta}{2} \right) E(\|\nabla F(w_k)\|_2^2) + \frac{L\eta^2\sigma^2}{2N_s B_s} \\
&\stackrel{(a)}{\leq} E(F(w_k)) - \frac{\eta}{2} E(\|\nabla F(w_k)\|_2^2) + \frac{L\eta^2\sigma^2}{2N_s B_s} \\
&\stackrel{(b)}{\leq} E(F(w_k)) - \eta c E(F(w_k) - F^*) + \frac{L\eta^2\sigma^2}{2N_s B_s}.
\end{aligned} \tag{22}$$

Here step (a) follows from  $\eta \leq \frac{1}{2L(\frac{\Theta}{N_s B_s} + 1)}$ , step (b) follows from  $2c(F(w) - F^*) \leq \|\nabla F(w)\|_2^2$ .

Therefore,

$$\begin{aligned}
E(F(w_{k+1}) - F^*) &\leq (1 - \eta c) E(F(w_k) - F^*) + \frac{L\eta^2\sigma^2}{2N_s B_s} \\
&\leq (1 - \eta c)^{k+1} \left( E(F(w_0) - F^*) - \frac{L\eta\sigma^2}{2cN_s B_s} \right) + \frac{L\eta\sigma^2}{2cN_s B_s}.
\end{aligned} \tag{23}$$

□

## B Workflows of GBA

In this section, we abstract the workflows of GBA. Algorithm 1 summarizes the workflow on workers in GBA. We implement pipeline between data downloading and data ingestion to accelerate the training. After completing the computation of gradients, the worker would directly send the gradient with the token back to the PS in a non-blocking way. In this way, the fast workers would ingest much more data than the stragglers. When a worker recovered from a failure, it would drop the previous state (e.g., data in the batch buffer and token) and proceed to deal with the new batch. The disappearance of a specific token would not change the correctness and efficiency of GBA.

---

### Algorithm 1 Workflow on workers

---

**Ensure:** Downloading threads: Download data asynchronously to a *download buffer*;  
Pack threads: Prepare the batch of data from the download buffer to a *batch buffer*;  
Computation threads: Execute the forward and backward pass of the model;  
Communication threads: Pull and push parameters by GRPC;

- 1: **Downloading threads**
- 2: **repeat**
- 3:   Get the addresses of a number of batches (data shard) from PS.
- 4:   **repeat**
- 5:     **if** The download buffer is not full **then**
- 6:       Download a batch of data.
- 7:     **else**
- 8:       Sleep 100ms.
- 9:     **end if**
- 10:   **until** All the data from this shard has been downloaded
- 11: **until** No more data shards to get
- 12:
- 13: **Computation threads**
- 14: **repeat**
- 15:   Get a batch from the batch buffer in a blocking way.
- 16:   Pull the parameters and fetch a token from PS.
- 17:   Compute the forward and backward pass.
- 18:   Send the local gradient and the token back to PS in a non-blocking way.
- 19: **until** No more data to ingest

---

Algorithm 2 summarizes the workflow on PSs in GBA. The token generation threads, the pull responding threads, and the push responding threads work asynchronously to avoid blocking of the

process. Different from the dense parameters, the embedding parameters are processed and updated by IDs, instead of by the entire embedding parameters. In practice, we optimize the memory usage as we could execute the weighted sum over some gradients in advance based on the tokens.

---

**Algorithm 2** Workflow on PSs

---

**Ensure:** Token generation thread: Generate tokens to the token list;  
 Pull responding threads: Send the parameters and a token to the worker;  
 Push responding threads: Receive the gradients from a worker and apply them if necessary.

- 1: **Token generation thread** (Only on PS 0, with lock)
- 2: **if** Successfully acquire the lock **then**
- 3:   **if** The number of tokens in the token list is less than the number of workers **then**
- 4:     Insert new tokens to the tail of the token list (a Queue)
- 5:   **end if**
- 6: **end if**
- 7:
- 8: **Pull responding threads**
- 9: Receive the request from a worker with the embedding IDs.
- 10: Look up the embedding tables based on the IDs for the embedding parameters.
- 11: Fetch a token from the token list and trigger the token generation thread (only on PS 0).
- 12: Send the parameters (and the token) back to the worker.
- 13:
- 14: **Push responding threads**
- 15: Receive the gradients from a worker.
- 16: Store the gradients with the token to the gradient buffer.
- 17: **if** At least  $N_a$  gradients are cached in the gradient buffer **then**
- 18:   Pop  $N_a$  gradients from the gradient buffer.
- 19:   Update the global step of appearance tagged to each ID.
- 20:   Decay the gradients of the dense parameters based on the current global step and the attached token.
- 21:   Decay the gradients of the embedding parameter based on the tagged global step of each ID and the attached token to the gradient.
- 22:   Calculate the weighted sum of the gradients of the dense parameters, divided by  $N_a$ .
- 23:   Calculate the weighted sum of the gradients of the embedding parameters, divided by the number of workers that encountered the particular ID.
- 24: **end if**

---

**C Detailed statistics of Table 6 in the submission**

Here we want to clarify the statements about Figure 6 in the submission, and present the detailed statistics. Table 6.1-6.3 depict the AUCs after inheriting the checkpoints trained via synchronous training. Table 6.5-6.7 introduce the AUCs after inheriting the checkpoints trained by the compared training modes and being switched to synchronous training. We collect the mean AUCs from the first day, the last day, and all days across the three datasets, as shown in Table 6.4 and Table 6.8. We can infer from the two tables that GBA provides the closest AUC scores as synchronous training. GBA appears with the lowest immediate AUC drop after switching, i.e., merely 0.1% decrement after switching from/to synchronous training at the first day. Throughout the three datasets, GBA outperforms the other baselines by at least 0.2% (Hop-BW in Table 6.4) when switching from synchronous training and 0.1% (Hop-BS in Table 6.8) when switching to synchronous training.

**D Proof of sudden drop in performance after switching.**

**Theorem 3.** *Based on the above Assumption and  $\frac{1}{NL(\frac{\sigma}{B}+1)} \leq \eta \leq \frac{1}{2L(\frac{\sigma}{B}+1)}$ , also suppose that for some  $\gamma \leq 1$ ,*

$$E\left(\|\nabla F(w_k) - \nabla F(w_{\tau(i,k)})\|_2^2\right) \leq \gamma E(\|\nabla F(w_k)\|_2^2),$$

*in the asynchronous training, the expectation of loss in the  $k + 1$  step is deduced by*

$$E(F(w_{k+1})) \leq E(F(w_k)) - \frac{\eta}{2}(1 - \gamma)E(\|\nabla F(w_k)\|_2^2) + \frac{L\eta^2\sigma^2}{2B} - \frac{\eta}{4}E(\|\nabla F(w_{\tau(k)})\|_2^2). \quad (24)$$

Table 6.1: Figure 6(a) - Criteo (from Sync.)

Date	Sync.	GBA	Hop-BW	Hop-BS	BSP	Aysnc.
13	0.7999	0.7964	0.7954	0.7924	0.7930	0.5000
14	0.7957	0.7932	0.7959	0.7869	0.7886	0.5000
15	0.7967	0.7957	0.7895	0.7891	0.7889	0.5000
16	0.7963	0.7956	0.7932	0.5040	0.7891	0.5000
17	0.7962	0.7955	0.7930	0.5040	0.7883	0.5000
18	0.7957	0.7950	0.7939	0.5030	0.7862	0.5000
19	0.7972	0.7966	0.7968	0.5030	0.7863	0.5000
20	0.7974	0.7973	0.7985	0.5030	0.7868	0.5000
21	0.7965	0.7959	0.7948	0.5050	0.7863	0.5000
22	0.7957	0.7955	0.7939	0.5040	0.7865	0.5000
23	0.7987	0.7986	0.7933	0.5060	0.7871	0.5000
Avg.	0.7969	0.7959	0.7944	0.5819	0.7879	0.5000

Table 6.2: Figure 6(b) - Alimama (from Sync.)

Date	Sync.	GBA	Hop-BW	Hop-BS	BSP	Aysnc.
6	0.6490	0.6489	0.6472	0.6488	0.6472	0.5000
7	0.6503	0.6502	0.6478	0.6503	0.6500	0.5000
8	0.6523	0.6523	0.6483	0.6523	0.6512	0.5000
Avg.	0.6505	0.6505	0.6478	0.6505	0.6495	0.5000

Table 6.3: Figure 6(c) - Private (from Sync.)

Date	Sync.	GBA	Hop-BW	Hop-BS	BSP	Aysnc.
15	0.7877	0.7880	0.7870	0.7875	0.7880	0.7795
16	0.7874	0.7877	0.7860	0.7878	0.7870	0.7785
17	0.7856	0.7860	0.7840	0.7858	0.7850	0.7774
18	0.7884	0.7888	0.7850	0.7882	0.7877	0.7873
19	0.7894	0.7905	0.7855	0.7890	0.7886	0.7878
20	0.7785	0.7788	0.7750	0.7781	0.7774	0.7598
21	0.7865	0.7868	0.7823	0.7863	0.7850	0.7769
22	0.7862	0.7870	0.7825	0.7858	0.7862	0.7754
Avg.	0.7862	0.7867	0.7834	0.7861	0.7856	0.7778

Table 6.4: Average AUC decrement on three datasets between GBA and the other baselines (from Sync.)

	Sync.	Hop-BW	Hop-BS	BSP	Aysnc.
1st day	+0.0011	-0.0012	-0.0015	-0.0017	-0.1513
last day	-0.0002	-0.0046	-0.0979	-0.0045	-0.1542
Average	+0.0002	-0.0025	-0.0716	-0.0034	-0.1518

Table 6.5: Figure 6(d) - Criteo (to Sync.)

Date	Sync.	GBA	Hop-BW	Hop-BS	BSP	Aysnc.
13	0.7999	0.7963	0.7968	0.7937	0.7913	0.7872
14	0.7957	0.7947	0.7933	0.7917	0.7907	0.7902
15	0.7967	0.7957	0.7952	0.7932	0.7923	0.7922
16	0.7963	0.7954	0.7956	0.7937	0.7944	0.7939
17	0.7962	0.7956	0.7946	0.7943	0.7945	0.7935
18	0.7957	0.7958	0.7949	0.7931	0.7922	0.7929
19	0.7972	0.7966	0.7960	0.7952	0.7944	0.7946
20	0.7974	0.7970	0.7970	0.7962	0.7957	0.7957
21	0.7965	0.7963	0.7956	0.7950	0.7931	0.7952
22	0.7957	0.7955	0.7955	0.7953	0.7940	0.7950
23	0.7987	0.7982	0.7978	0.7973	0.7964	0.7972
Avg.	0.7969	0.7961	0.7957	0.7944	0.7935	0.7934

Table 6.6: Figure 6(e) - Alimama (to Sync.)

Date	Sync.	GBA	Hop-BW	Hop-BS	BSP	Aysnc.
6	0.6490	0.6492	0.6401	0.6484	0.6452	0.6352
7	0.6503	0.6504	0.6437	0.6499	0.6487	0.6426
8	0.6523	0.6523	0.6471	0.6520	0.6503	0.6456
Avg.	0.6505	0.6506	0.6436	0.6501	0.6481	0.6411

Table 6.7: Figure 6(f) - Private (to Sync.)

Date	Sync.	GBA	Hop-BW	Hop-BS	BSP	Aysnc.
15	0.7877	0.7878	0.7783	0.7859	0.7732	0.7870
16	0.7874	0.7877	0.7844	0.7867	0.7767	0.5000
17	0.7856	0.7855	0.7813	0.7853	0.7782	0.5000
18	0.7884	0.7883	0.7858	0.7880	0.7805	0.5000
19	0.7894	0.7896	0.7870	0.7889	0.7848	0.5000
20	0.7785	0.7786	0.7761	0.7784	0.7746	0.5000
21	0.7865	0.7865	0.7843	0.7864	0.7828	0.5000
22	0.7862	0.7863	0.7855	0.7861	0.7838	0.5000
Avg.	0.7862	0.7863	0.7828	0.7857	0.7793	0.5359

Table 6.8: Average AUC decrement on three datasets between GBA and the other baselines (to Sync.)

	Sync.	Hop-BW	Hop-BS	BSP	Aysnc.
1st day	+0.0011	-0.0060	-0.0018	-0.0079	-0.0080
last day	+0.0001	-0.0021	-0.0005	-0.0021	-0.0980
Average	+0.0002	-0.0036	-0.0009	-0.0040	-0.0875

If we switch to the **synchronous training** in the  $k + 1$  step, the expectation of loss is shown as follows

$$\begin{aligned} E(F(w_{k+1})) &\leq E(F(w_k)) - \frac{\eta}{2}(1 - \gamma)E(\|\nabla F(w_k)\|_2^2) + \frac{L\eta^2\sigma^2}{2B} + \frac{L\eta^2\sigma^2}{2BN} \\ &\quad + \left(\frac{L\eta^2\Theta}{2B} + \frac{L\eta^2}{2} - \frac{\eta}{2N}\right)E(\|\nabla F(w_k)\|_2^2) - \frac{\eta}{4N}E(\|\nabla F(w_{\tau(k)})\|_2^2) \end{aligned} \quad (25)$$

and switching the asynchronous mode to the synchronous mode may drop in performance.

*proof of Theorem 3.* According to Theorem 1, (24) could be obtained if we apply the asynchronous training mode. Next, we will prove (25).

Let  $w_{k+1} = w_k - \eta v_k$ ,  $v_k = \frac{1}{N} \sum_{i=1}^N g(w_{\tau(i,k)})$ , we have

$$\begin{aligned} F(w_{k+1}) &\leq F(w_k) + (w_{k+1} - w_k)^T \nabla F(w_k) + \frac{L}{2} \|w_{k+1} - w_k\|_2^2 \\ &\leq F(w_k) + \langle -\eta v_k, \nabla F(w_k) \rangle + \frac{L}{2} \eta^2 \|v_k\|_2^2 \\ &= F(w_k) - \frac{\eta}{N} \sum_{i=1}^N \langle g(w_{\tau(i,k)}), \nabla F(w_k) \rangle + \frac{L}{2} \eta^2 \|v_k\|_2^2. \end{aligned} \quad (26)$$

Since we switch the asynchronous training to the synchronous training, the gradient of each worker  $g(w_{\tau(i,k)})$ ,  $i = 1, 2, \dots, N$ , in the  $k$  step may be different.

Owing to  $2\langle x, y \rangle = \|x\|_2^2 + \|y\|_2^2 - \|x - y\|_2^2$ , the expectation of (26) is shown as follows,

$$\begin{aligned} E(F(w_{k+1})) &\leq E(F(w_k)) - \frac{\eta}{2}E(\|\nabla F(w_k)\|_2^2) - \frac{\eta}{2N} \sum_{i=1}^N E(\|g(w_{\tau(i,k)})\|_2^2) \\ &\quad + \frac{\eta}{2N} \sum_{i=1}^N E(\|g(w_{\tau(i,k)}) - \nabla F(w_k)\|_2^2) + \frac{L}{2} \eta^2 E(\|v_k\|_2^2). \end{aligned} \quad (27)$$

Since there applied a gradient in the  $k$  step of the asynchronous training, we may assume  $g(w_{\tau(1,k)}) = g(w_k)$ . Hence,

$$\begin{aligned} &\frac{\eta}{2N} \sum_{i=1}^N E(\|g(w_{\tau(i,k)}) - \nabla F(w_k)\|_2^2) \\ &= \frac{\eta}{2N} \left( E(\|g(w_{\tau(1,k)}) - \nabla F(w_k)\|_2^2) + \sum_{j=2}^N E(\|g(w_{\tau(j,k)}) - \nabla F(w_k)\|_2^2) \right) \\ &= \frac{\eta}{2N} \left( E(\|g(w_k)\|_2^2) - E(\|\nabla F(w_k)\|_2^2) \right) \\ &\quad + \frac{\eta}{2N} \sum_{j=2}^N \left( E(\|g(w_{\tau(j,k)})\|_2^2) - E(\|\nabla F(w_{\tau(j,k)})\|_2^2) + E(\|\nabla F(w_{\tau(j,k)}) - \nabla F(w_k)\|_2^2) \right) \end{aligned} \quad (28)$$

Besides,

$$\frac{\eta}{2N} \sum_{i=1}^N E(\|g(w_{\tau(i,k)})\|_2^2) = \frac{\eta}{2N} E(\|g(w_k)\|_2^2) + \frac{\eta}{2N} \sum_{j=2}^N E(\|g(w_{\tau(j,k)})\|_2^2). \quad (29)$$

Based on (28) and (29), we have

$$\begin{aligned}
E(F(w_{k+1})) &\leq E(F(w_k)) - \frac{\eta}{2}E(\|\nabla F(w_k)\|_2^2) - \frac{\eta}{2N}E(\|\nabla F(w_k)\|_2^2) + \frac{L}{2}\eta^2E(\|v_k\|_2^2) \\
&\quad - \frac{\eta}{2N}\sum_{j=2}^NE(\|\nabla F(w_{\tau(j,k)})\|_2^2) + \frac{\eta}{2N}\sum_{j=2}^NE(\|\nabla F(w_{\tau(j,k)}) - \nabla F(w_k)\|_2^2) \\
&\stackrel{(a)}{\leq} E(F(w_k)) - \frac{\eta}{2}E(\|\nabla F(w_k)\|_2^2) - \frac{\eta}{2N}E(\|\nabla F(w_k)\|_2^2) + \frac{L}{2}\eta^2E(\|v_k\|_2^2) \\
&\quad - \frac{\eta}{2N}\sum_{j=2}^NE(\|\nabla F(w_{\tau(j,k)})\|_2^2) + \frac{\gamma\eta}{2}E(\|\nabla F(w_k)\|_2^2) \\
&= E(F(w_k)) - \frac{\eta}{2}(1-\gamma)E(\|\nabla F(w_k)\|_2^2) - \frac{\eta}{2N}E(\|\nabla F(w_k)\|_2^2) + \frac{L}{2}\eta^2E(\|v_k\|_2^2) \\
&\quad - \frac{\eta}{2N}\sum_{j=2}^NE(\|\nabla F(w_{\tau(j,k)})\|_2^2).
\end{aligned} \tag{30}$$

Here, step (a) follows from  $E(\|\nabla F(w_k) - \nabla F(w_{\tau(j,k)})\|_2^2) \leq \gamma E(\|\nabla F(w_k)\|_2^2)$ .

$$\begin{aligned}
E(\|v_k\|_2^2) &= E\left(\left\|\frac{1}{N}\sum_{i=1}^Ng(w_{\tau(i,k)})\right\|_2^2\right) = \frac{1}{N^2}E\left(\left\|\sum_{i=1}^Ng(w_{\tau(i,k)})\right\|_2^2\right) \\
&= \frac{1}{N^2}E\left(\left\|\sum_{i=1}^Ng(w_{\tau(i,k)}) - \nabla F(w_{\tau(i,k)}) + \nabla F(w_{\tau(i,k)})\right\|_2^2\right) \\
&= \frac{1}{N^2}E\left(\left\|\sum_{i=1}^Ng(w_{\tau(i,k)}) - \nabla F(w_{\tau(i,k)})\right\|_2^2\right) + \frac{1}{N^2}E\left(\left\|\sum_{i=1}^N\nabla F(w_{\tau(i,k)})\right\|_2^2\right) \\
&\leq E\left(\|g(w_k) - \nabla F(w_k)\|_2^2\right) + \frac{1}{N^2}\sum_{j=2}^NE\left(\|g(w_{\tau(j,k)}) - \nabla F(w_{\tau(j,k)})\|_2^2\right) \\
&\quad + E\left(\|\nabla F(w_k)\|_2^2\right) + \frac{1}{N}\sum_{j=2}^NE\left(\|\nabla F(w_{\tau(j,k)})\|_2^2\right) \\
&\leq \frac{\sigma^2}{B} + \frac{\Theta}{B}E\left(\|\nabla F(w_k)\|_2^2\right) + \frac{1}{N^2}\sum_{j=2}^N\left(\frac{\sigma^2}{B} + \frac{\Theta}{B}E\left(\|\nabla F(w_{\tau(j,k)})\|_2^2\right)\right) \\
&\quad + E\left(\|\nabla F(w_k)\|_2^2\right) + \frac{1}{N}\sum_{j=2}^NE\left(\|\nabla F(w_{\tau(j,k)})\|_2^2\right)
\end{aligned} \tag{31}$$

Based on (31), we obtain

$$\begin{aligned}
E(F(w_{k+1})) &\leq E(F(w_k)) - \frac{\eta}{2}(1-\gamma)E(\|\nabla F(w_k)\|_2^2) + \frac{L\eta^2\sigma^2}{2B} + \frac{L\eta^2\sigma^2}{2BN} \\
&\quad + \left(\frac{L\eta^2\Theta}{2B} + \frac{L\eta^2}{2} - \frac{\eta}{2N}\right)E\left(\|\nabla F(w_k)\|_2^2\right) \\
&\quad + \sum_{j=2}^N\left(\frac{L\eta^2\Theta}{2BN^2} + \frac{L\eta^2}{2N} - \frac{\eta}{2N}\right)E\left(\|\nabla F(w_{\tau(j,k)})\|_2^2\right).
\end{aligned} \tag{32}$$

In (32),

$$\begin{aligned}
&\sum_{j=2}^N\left(\frac{L\eta^2\Theta}{2BN^2} + \frac{L\eta^2}{2N} - \frac{\eta}{2N}\right)E\left(\|\nabla F(w_{\tau(j,k)})\|_2^2\right) \\
&= \frac{\eta}{2N}\sum_{j=2}^N\left(\frac{L\eta\Theta}{BN} + L\eta - 1\right)E\left(\|\nabla F(w_{\tau(j,k)})\|_2^2\right) \leq -\frac{\eta}{4N}E\left(\|\nabla F(w_{\tau(k)})\|_2^2\right).
\end{aligned} \tag{33}$$

Therefore,

$$\begin{aligned}
E(F(w_{k+1})) &\leq E(F(w_k)) - \frac{\eta}{2}(1-\gamma)E(\|\nabla F(w_k)\|_2^2) + \frac{L\eta^2\sigma^2}{2B} + \frac{L\eta^2\sigma^2}{2BN} \\
&\quad + \left(\frac{L\eta^2\Theta}{2B} + \frac{L\eta^2}{2} - \frac{\eta}{2N}\right)E(\|\nabla F(w_k)\|_2^2) - \frac{\eta}{4N}E(\|\nabla F(w_{\tau(k)})\|_2^2)
\end{aligned} \tag{34}$$

Owing to  $\eta \geq \frac{1}{NL(\frac{\Theta}{B}+1)}$ , we have  $\frac{L\eta\Theta}{B} + L\eta \geq \frac{1}{N}$  and

$$\left(\frac{L\eta^2\Theta}{2B} + \frac{L\eta^2}{2} - \frac{\eta}{2N}\right)E(\|\nabla F(w_k)\|_2^2) = \frac{\eta}{2}\left(\frac{L\eta\Theta}{B} + L\eta - \frac{1}{N}\right)E(\|\nabla F(w_k)\|_2^2) \geq 0. \tag{35}$$

Since  $-\frac{\eta}{4N}E(\|\nabla F(w_{\tau(k)})\|_2^2) > -\frac{\eta}{4}E(\|\nabla F(w_{\tau(k)})\|_2^2)$ , we have

$$\begin{aligned}
E(F(w_k)) &- \frac{\eta}{2}(1-\gamma)E(\|\nabla F(w_k)\|_2^2) + \frac{L\eta^2\sigma^2}{2B} - \frac{\eta}{4}E(\|\nabla F(w_{\tau(k)})\|_2^2) \\
&\leq E(F(w_k)) - \frac{\eta}{2}(1-\gamma)E(\|\nabla F(w_k)\|_2^2) + \frac{L\eta^2\sigma^2}{2B} + \frac{L\eta^2\sigma^2}{2BN} \\
&\quad + \left(\frac{L\eta^2\Theta}{2B} + \frac{L\eta^2}{2} - \frac{\eta}{2N}\right)E(\|\nabla F(w_k)\|_2^2) - \frac{\eta}{4N}E(\|\nabla F(w_{\tau(k)})\|_2^2).
\end{aligned} \tag{36}$$

Therefore, switching the asynchronous mode to the synchronous mode in the  $k+1$  step may drop in performance.  $\square$

**Theorem 4.** *Based on the above Assumption and  $\eta \leq \frac{1}{2L(\frac{\Theta}{B}+1)}$ , in the synchronous training, the expectation of loss in the  $k+1$  step is deduced by*

$$E(F(w_{k+1})) \leq E(F(w_k)) - \eta \left(1 - \frac{L\eta\Theta}{2NB} - \frac{L\eta}{2}\right) E(\|\nabla F(w_k)\|_2^2) + \frac{L\eta^2\sigma^2}{2NB}. \tag{37}$$

If we switch to the asynchronous training in the  $k+1$  step, the expectation of loss becomes as follows

$$E(F(w_{k+1})) \leq E(F(w_k)) - \eta \left(1 - \frac{L\eta\Theta}{2B} - \frac{L\eta}{2}\right) E(\|\nabla F(w_k)\|_2^2) + \frac{L\eta^2\sigma^2}{2B}, \tag{38}$$

and switching the synchronous mode to the asynchronous mode may drop in performance.

*proof of Theorem 4.* According to the Theorem 2, (37) could be obtained. Next, we will prove (38).

$$\begin{aligned}
E(F(w_{k+1})) &\leq E(F(w_k)) - \frac{\eta}{2}E(\|\nabla F(w_k)\|_2^2) - \frac{\eta}{2}E(\|g(w_{\tau(1,k)})\|_2^2) \\
&\quad + \frac{\eta}{2}E(\|g(w_{\tau(1,k)}) - \nabla F(w_k)\|_2^2) + \frac{L}{2}\eta^2E(\|v_k\|_2^2).
\end{aligned} \tag{39}$$

Since  $E(\|g(w_{\tau(1,k)}) - \nabla F(w_k)\|_2^2) = E(\|g(w_k)\|_2^2) - E(\|\nabla F(w_k)\|_2^2)$ , we have

$$E(F(w_{k+1})) \leq E(F(w_k)) - \eta E(\|\nabla F(w_k)\|_2^2) + \frac{L\eta^2}{2}E(\|v_k\|_2^2).$$

Owing to

$$\begin{aligned}
E(\|v_k\|_2^2) &= E(\|g(w_{\tau(1,k)})\|_2^2) = E(\|g(w_{\tau(1,k)}) - \nabla F(w_k) + \nabla F(w_k)\|_2^2) \\
&= E(\|g(w_{\tau(1,k)}) - \nabla F(w_k)\|_2^2) + E(\|\nabla F(w_k)\|_2^2) \\
&\leq \frac{\sigma^2}{B} + \left(\frac{\Theta}{B} + 1\right)E(\|\nabla F(w_k)\|_2^2),
\end{aligned} \tag{40}$$

we obtain

$$E(F(w_{k+1})) \leq E(F(w_k)) - \eta \left(1 - \frac{L\eta}{2} - \frac{L\eta\Theta}{2B}\right) E(\|\nabla F(w_k)\|_2^2) + \frac{L\eta^2\sigma^2}{2B}. \tag{41}$$



Owing to  $\frac{L\eta^2\sigma^2}{2B} > \frac{L\eta^2\sigma^2}{2NB}$  and  $\frac{L\eta\Theta}{2B} > \frac{L\eta\Theta}{2NB}$ , we have

$$\begin{aligned} & E(F(w_k)) - \eta \left( 1 - \frac{L\eta\Theta}{2NB} - \frac{L\eta}{2} \right) E(\|\nabla F(w_k)\|_2^2) + \frac{L\eta^2\sigma^2}{2NB} \\ & \leq E(F(w_k)) - \eta \left( 1 - \frac{L\eta\Theta}{2B} - \frac{L\eta}{2} \right) E(\|\nabla F(w_k)\|_2^2) + \frac{L\eta^2\sigma^2}{2B}. \end{aligned} \tag{42}$$

Hence, switching the synchronous mode to the asynchronous mode may drop in performance.  $\square$